

## Study on Corrosion Inhibition Performance of 1,2-Dithiolane-3-pentanoic acid on X65 Steel in 0.5 M Sulfuric Acid

Shiying Tao<sup>1,2,\*</sup>, Hui Huang<sup>3,\*</sup>

<sup>1</sup>Faculty of Science and Engineering, The University of Nottingham Ningbo China, Ningbo 315100, P R China

<sup>2</sup>Ningbo Nottingham New Materials Institute Ltd., Ningbo 315040, P R China

<sup>3</sup>School of Materials and Chemical Engineering, Ningbo University of Technology, Ningbo 315211, P R China

\*E-mail: [sy tao\\_nbu@163.com](mailto:sy tao_nbu@163.com), [Carey.Tao@nottingham.edu.cn](mailto:Carey.Tao@nottingham.edu.cn), [huihuang@nbut.edu.cn](mailto:huihuang@nbut.edu.cn)

Received: 12 February 2019 / Accepted: 7 April 2019 / Published: 10 May 2019

---

1,2-Dithiolane-3-pentanoic acid (DLP) has been tested for corrosion inhibition properties of X65 steel using a variety of experimental methods at 298 K in 0.5 M H<sub>2</sub>SO<sub>4</sub>. Electrochemical methods include classical polarization curves and electrochemical impedance spectroscopy. Electrochemical tests show that DLP can effectively inhibit the corrosion of X65 steel, and it is a mixed-type corrosion inhibitor. Morphological tests include atomic force microscopy and scanning electron microscopy. The morphology test results are highly consistent with the electrochemical experiments. In addition, quantum chemical calculations and molecular dynamics simulations were used to calculate DLP. Both experimental and theoretical results show that DLP exhibits excellent corrosion inhibition performance for X65 steel. The adsorption of DLP on the surface of X65 steel is consistent with Langmuir adsorption. And adsorbed on the surface of X65 by physicochemical adsorption.

---

**Keywords:** Corrosion inhibitor, X65 steel, Electrochemical method, Atomic force microscope, Scanning electron microscope, Theoretical calculation

### 1. INTRODUCTION

Metal corrosion is a spontaneous and irreversible process, causes great damage to metal materials, and the number of economic losses caused is staggering by metal corrosion in the world [1-6]. In addition, metal corrosion brings many potential dangers to human production and life safety. Therefore, how to effectively suppress the problem of metal has become a hot issue for anti-corrosion researchers since the moment the metal was put into human using. So far, effective measures for metal protection have been formed via many sophisticated means. The most common means include the following: (1) Modifying the substrate of the metal itself to effectively improve the corrosion resistance

of the metal, such as alloys, etc. (2) The surface treatment method forms an effective barrier layer on the surface of the metal to isolate the metal from the corrosive medium. Thereby the metal is effectively protected. This method includes coating and adding corrosion inhibitors, etc. (3) Electrochemical protection method, which uses an external current to change the electrode potential of a metal, thereby preventing metal corrosion, including cathode protection and anode protection.

Among these protection methods, the method of adding corrosion inhibitor is the easiest to operate, it is very convenient to use, the price is low, and the technology is mature, which has made it pay great attention to corrosion protection workers in metal protection [7]. Generally speaking, corrosion inhibitors include organic and inorganic corrosion inhibitors. Inorganic organics generally have fatal defects, such as large amounts of use and serious pollution to the ecological environment. Relatively speaking, the advantages of organic corrosion inhibitors are particularly obvious. For example, the amount of organic corrosion inhibitors is small. Due to the wide variety of organic corrosion inhibitors, a large number of environmentally-friendly slow release agents can be found, such as plants extraction[8], food spices[9, 10], etc.

X65 steel is widely used as a pipeline steel for natural gas and petroleum pipelines [11]. However, it is very susceptible to corrosion due to prolonged immersion in corrosive media. Therefore, it is especially important to use organic corrosion inhibitors to protect them. The organic corrosion inhibitor molecule contains some conjugated groups, heteroatoms, etc[3, 12, 13]. 1,2-Dithiolane-3-pentanoic acid contains sulfur and oxygen atoms, so it has potential as a corrosion inhibitor. On the other hand, in recent years, drugs as corrosion inhibitors have become more popular, due to the relatively small negative impact of drugs on the environment. For example, Tan et al [14]. studied the inhibitory effect of montelukast sodium, an asthma drug on copper in sulfuric acid. Gong et al [1]. studied the antifungal drug itraconazole to exhibit excellent corrosion inhibition properties of copper in sulfuric acid. Zhang et al [15]. combined experimental and theoretical methods to find the inhibitory effect of tri-anthracene, a hepatitis drug on copper in sulfuric acid. In this study, DL-Thioctic acid was used as a vitamin drug, which can be used to treat chronic hepatitis, diabetes, and cirrhosis. Through electrochemical methods, surface morphology analysis and theoretical calculations, it was found that 1,2-Dithiolane-3-pentanoic acid exhibited excellent corrosion inhibition performance in X65 steel in sulfuric acid corrosion medium.

## 2. EXPERIMENTAL

### 2.1 Material preparation

DLP purchased from Titan Reagent, no further purification of using. Its pure is 98.5%. The chemical formula is presented in Fig. 1. The 0.5 M sulfuric acid solution used as corrosion blank solution. The blank solution was used to prepare a test solution containing 1, 2, 3, 4, 5 mM DLP, respectively. The composition of X65 steel is shown in Table 1. It is made to contain a 1 x 1 cm<sup>2</sup> working surface and the other parts are completely sealed. X65 steel cut into two samples of 0.8×0.8×0.1cm<sup>3</sup> and 0.3×0.3×0.3 cm<sup>3</sup>, respectively. They were used in the tests of atomic force microscopy (MFP-3D-BIO) and scanning

electron microscopy (JEOL-JSM-7800F). Polish all X65 samples on 180 to 5000 sandpaper before testing. The polished samples were immersed in 5 mM sulfuric acid and a blank solution for 2 hours at 25 °C. After the steel surface was cleaned, AFM and SEM tests were performed.

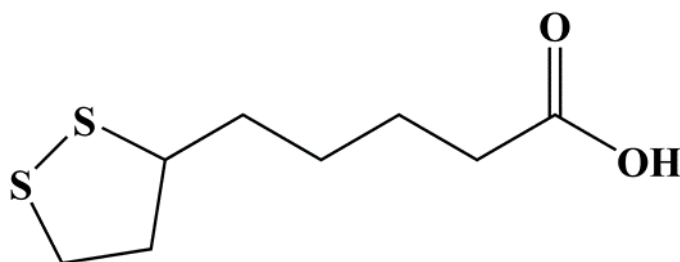


**Figure 1.** Molecular formula of 1,2-Dithiolane-3-pentanoic acid.

**Table 1.** Chemical composition of X65 steel

| Elements   | Fe      | Mn    | Si    | Cr    | C     | Nb     | Al     |
|------------|---------|-------|-------|-------|-------|--------|--------|
| Proportion | 97.894% | 1.64% | 0.17% | 0.16% | 0.06% | 0.041% | 0.035% |

## 2.2 Theoretical calculation details

Quantum chemical calculation of DLP molecule was performed on Material Studio 8.0 software. The calculated parameter settings are as follows: The task of calculation is structural optimization. Quality is fine. Energy is  $3 \times 10^{-5}$  Ha. Max.force is 0.04 Ha/Å. Basis Set is DNP. Basis file is 4.4. Forcefield is the COMPASS force field. After optimizing the DL-Thioctic acid molecule, the dipole moment, the energy of the HOMO and LUMO orbitals are separately counted. The adsorption behavior of DL-Thioctic acid molecules and 300 water molecules on the Fe(110) surface was then simulated in the Forcite module of MS software. The parameters are set as follows: the calculated task is Dynamics. Qualit is fine. Ensemble is NVT. Time step is 1fs, and Total simulation time is 300ps.

## 2.3 Electrochemical test

Electrochemical experiments were tested using a three-electrode system on the Chi604D electrochemical workstation. Among them, X65 steel is used as the working electrode, platinum electrode is used as the counter electrode, and saturated calomel electrode is used as the reference electrode. The entire electrochemical test was performed in a 150 mL beaker. Ensure that the test system is connected to the atmosphere. The test solution is 100 mL to ensure that the entire working system is completely immersed in corrosive media. First, we tested the open circuit potential to ensure that the steel electrode reached a stable state in the corrosive solution. The open test time is set to 1200s. Next, the impedance spectrum is tested. The initial voltage is a stable open circuit voltage. The tested frequency range is 100000 Hz to 0.01 Hz. The disturbance signal is a sine wave with an amplitude of 5 mV. Finally, the potentiodynamic polarization curve was tested. The range of polarization was from  $E_{OCP} \pm 250$  mV and the test rate was 1 mV/s [16].

### 3. RESULTS AND DISCUSSION

#### 3.1 Potentiodynamic polarization curves

Fig. 2 shows the potentiodynamic polarization curves of the X65 electrode in the presence and absence of DLT. It can be seen from Fig. 2 that as the concentration of DLP increases, the corrosion current density decreases sharply, and the rate of decrease is proportional to the concentration of the inhibitor. This indicates that DLP forms a protective film on the surface of the steel electrode to effectively inhibit corrosion of the steel. In addition, the corrosion potential is obviously shifted toward the anode, which indicates that the inhibition effect of DLP on the dissolution of anode iron is greater than that of cathode hydrogen reduction.

DLP forms a coordination bond with the 3d orbital of Fe through the lone pair of electrons in the S atom, thereby effectively adsorbing on the surface of X65, reducing the contact area between X65 steel and corrosive medium. It is worth mentioning that the polarization curves of the cathodes show a parallel trend, which indicates that the adsorption of DLP does not have a mechanism of cathode reaction.

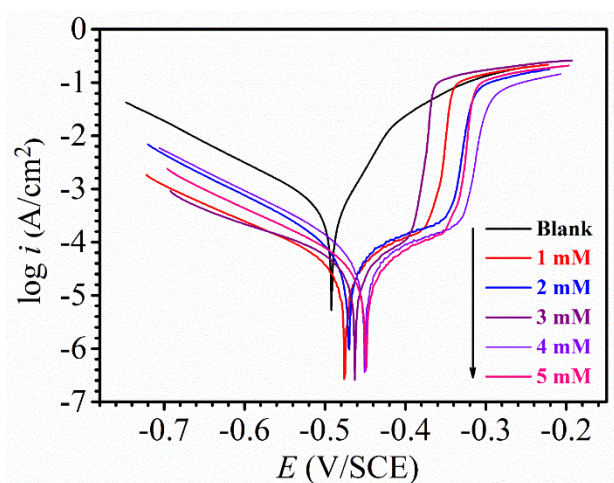


**Figure 2.** The potentiodynamic polarization curves of the X65 electrode in the presence and absence of different concentrations DLP in 298 K.

Table 2 is the electrochemical parameters obtained by the polarization curve. Corrosion potential, corrosion current density and Taf slope of cathode and anode can be obtained by Taf extrapolation. The formula for calculating the corrosion inhibition efficiency is as following [17-20]:

$$\eta(\%) = \frac{I_{corr,0} - I_{corr}}{I_{corr,0}} \times 100 \quad (1)$$

From Table 2, it can be found that the corrosion potential of X65 in the blank solution is  $-0.48$  V. After adding 5 mM DLP, the corrosion potential became  $-0.44$  V and moved 44 mV toward the anode. It is well known that when the corrosion potential moves over 85 mV with respect to the blank solution, it can be considered as a cathode type or anode corrosion inhibitor [21]. Therefore, it can be judged that DLP is a mixed-type corrosion inhibitor. When the concentration of DLP is 5 mM, the

inhibition efficiency is 90.7%. Therefore, the corrosion of X65 in the sulfuric acid solution can be effectively suppressed.

**Table 2.** Electrochemical parameters obtained from polarization curves.

| C (mM)     | $E_{corr}$ (V/SCE) | $I_{corr}$ ( $\mu\text{A cm}^{-2}$ ) | $\beta_c$ (mV dec $^{-1}$ ) | $\beta_a$ (mV dec $^{-1}$ ) | $\eta$ (%) |
|------------|--------------------|--------------------------------------|-----------------------------|-----------------------------|------------|
| Blank      | -0.48              | 267.1                                | -114                        | 74                          | —          |
| <b>DLP</b> |                    |                                      |                             |                             |            |
| 1          | -0.48              | 37.6                                 | -97                         | 99                          | 85.9       |
| 2          | -0.47              | 35.0                                 | -100                        | 97                          | 86.9       |
| 3          | -0.46              | 31.7                                 | -101                        | 97                          | 88.1       |
| 4          | -0.45              | 28.3                                 | -105                        | 98                          | 89.4       |
| 5          | -0.44              | 24.8                                 | -103                        | 95                          | 90.7       |

### 3.2 Electrochemical impedance spectroscopy

Fig. 3 is the Nyquist plot of X65 steel in 0.5 M sulfuric acid containing and lacking DLP at 298 K. It can be clearly found that the radius of the capacitive arc becomes significantly larger as the concentration of DLP increases, which indicates that DLP forms a dense protective film on the surface of X65, thereby increasing the charge transfer resistance. In addition, it is worth mentioning that the capacitive reactance arc presents a flattened semicircle due to the adsorption of the DLP and the erosion of the sulfuric acid corrosive medium resulting in electrode inhomogeneity [22].

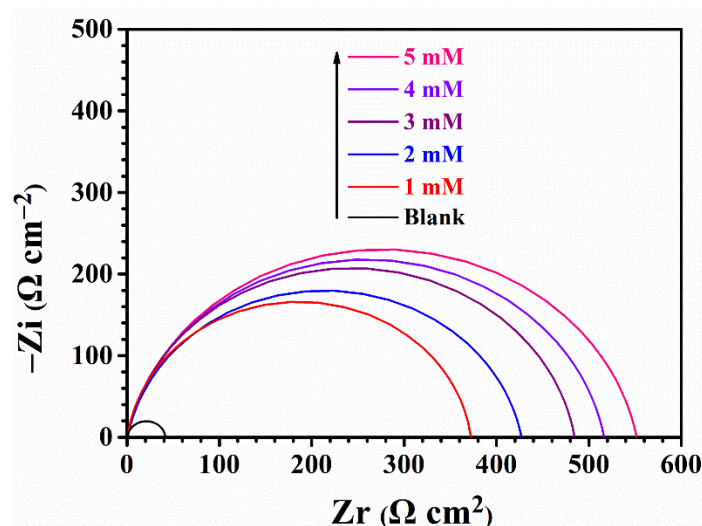


**Figure 3.** The Nyquist plot of X65 steel in 0.5 M sulfuric acid at 298 K in the presence and absence of different concentrations DLP.

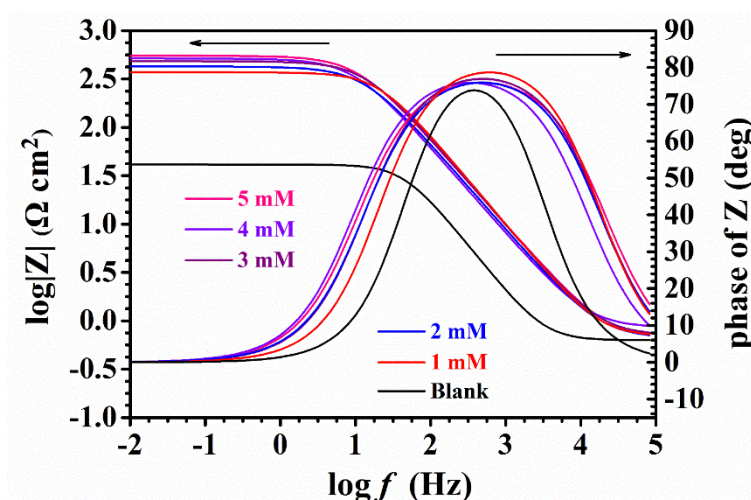


**Figure 4.** The Bode diagram of X65 steel in 0.5 M sulfuric acid at 298 K in the presence and absence of different concentrations DLP.

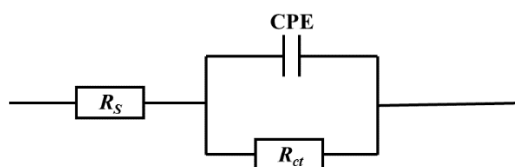


**Figure 5.** Equivalent circuit for fitting the impedance spectrum.

Fig. 4 is the Bode diagram of X65 steel in 0.5 M sulfuric acid containing and lacking DLP. It can be seen from the diagram that the impedance modulus of the low frequency region is increased by an order of magnitude relative to the blank solution when DLP is present. In addition, as the concentration of DLP increases, the phase angle map is significantly wider in the high frequency region than the blank solution. Only one peak appeared in the phase angle diagram, indicating that only one time constant appeared during this reaction due to the adsorption of DLP on the surface of the X65 steel. The most worthwhile mention is that the slope of  $\log|Z|$  vs  $\log f$  is 1, which indicates that the surface of the electrode produces capacitive behavior. These all indicate that DLP can effectively inhibit the corrosion of X65 steel in sulfuric acid solution.

In order to quantitatively analyze the electrochemical parameters in the impedance spectrum, the equivalent circuit diagram of Fig. 5 was used to fit the EIS data. The chi-squared values after fitting are all less than  $10^{-3}$ , which indicates that the error between the experimental value and the fitted value is small. As shown in Fig. 5,  $R_s$  represents the solution resistance,  $R_{ct}$  represents the charge transfer resistance, and  $CPE$  represents the constant phase angle element. The fitted values are listed in Table 3, where  $R_s$  represents the solution resistance and  $R_{ct}$  is the charge transfer resistance.  $C_{dl}$  represents the electric double layer capacitance, and  $n$  indicates the deviation index, wherein the corrosion inhibition efficiency can be obtained by the following formula [23, 24]:

$$\eta(\%) = \frac{R_{ct} - R_{ct,0}}{R_{ct}} \times 100 \quad (2)$$

where  $R_{ct}$  and  $R_{ct,0}$  indicate charge transfer resistance in the presence of DLP and blank solution, respectively. In addition, the expressions of  $CPE$  and  $C_{dl}$  are as follows[25-27]:

$$Z_{CPE} = \frac{1}{Y_0(j\omega)^n} \quad (3)$$

$$C = Y_0(\omega)^{n-1} = Y_0(2\pi f_{Z_{im-Max}})^{n-1} \quad (4)$$

It can be seen from Table 3 that as the concentration of DLT increases, the value of  $n$  increases continuously and approaches unit 1, which indicates that DLP forms a dense protective film in steel, resulting in the properties of capacitance [28]. In addition, the value of  $C_{dl}$  in the blank solution was  $97.37\mu\text{F cm}^{-2}$ , and when the concentration of DLP was 5 mM, the value of  $C_{dl}$  decreased to  $21.4\mu\text{F cm}^{-2}$ . This is due to the fact that the DLP molecule replaces the molecules on the steel surface.

**Table 3.** Electrochemical parameters after fitting of electrochemical impedance spectroscopy.

| C (mM)     | $R_s$ ( $\Omega\text{ cm}^2$ ) | $Y_0 \times 10^{-6}$ ( $\text{S s}^n\text{ cm}^{-2}$ ) | $n$  | $C_{dl}$ ( $\mu\text{F cm}^{-2}$ ) | $R_{ct}$ ( $\Omega\text{ cm}^2$ ) | $\eta$ (%) |
|------------|--------------------------------|--|------|------------------------------------|-----------------------------------|------------|
| Blank      | 0.5                            | 181.6  | 0.89 | 97.37                              | 40.9                              | -          |
| <b>DLP</b> |                                |  |      |                                    |                                   |            |
| 1          | 0.5                            | 67.9   | 0.91 | 36.9                               | 371.8                             | 88.9       |
| 2          | 0.7                            | 68.3   | 0.94 | 34.7                               | 426.3                             | 90.4       |
| 3          | 0.8                            | 61.0   | 0.97 | 31.4                               | 483.4                             | 91.5       |
| 4          | 0.8                            | 69.3   | 0.98 | 25.1                               | 510.0                             | 91.9       |
| 5          | 0.9                            | 68.7   | 0.99 | 21.4                               | 551.1                             | 92.6       |

### 3.3 Adsorption isotherm model study

The adsorption isotherm model study can help to understand the adsorption of corrosion inhibitor molecules on the surface of X65 steel. We used polarization curve data to fit different isothermal adsorption equations. The linear regression coefficient indicates the adsorption behavior of DLP on the surface of X65 steel, which is consistent with the Langmuir adsorption isotherm. Its expression is as follows [29-31]:

$$\frac{\theta}{1-\theta} = K_{ads}C \quad (5)$$

Among them,  $\theta$  is obtained by the corrosion inhibition efficiency,  $K_{ads}$  represents the adsorption equilibrium constant, and  $C$  is the concentration of DLP. In order to further judge the type of adsorption of DLP on the steel surface. The value of  $\Delta G_{ads}^0$  is calculated as follows[24]:

$$K_{ads} = \frac{1}{55.5} \exp\left(-\frac{\Delta G_{ads}^0}{RT}\right) \quad (6)$$

The calculated values ( $\Delta G_{ads}^0$  and  $K_{ads}$ ) are presented in Fig. 6, respectively. It is well known that large  $K_{ads}$  values and small  $\Delta G_{ads}^0$  values indicate that DLP exhibits excellent corrosion inhibition

properties on the surface of X65 steel. In addition, the values are between  $-20$  kJ/mol and  $-40$  kJ/mol [32, 33]. It indicates that DLP has both physical and chemical adsorption on the surface of X65 steel.

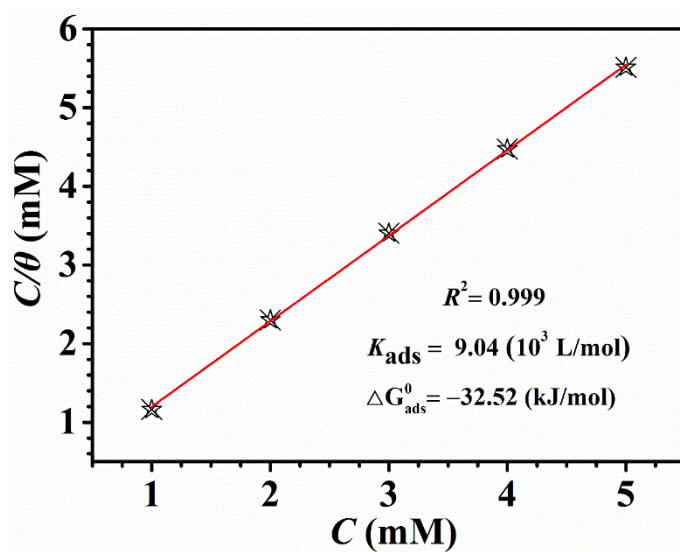


**Figure 6.** Langmuir adsorption isotherm of DLP on X65 surface

### 3.4 Scanning electron microscopy analysis

Fig. 7 is a surface topography diagram of X65 under different processing conditions. Fig.7 (a), (b) and (c) are the topographical map of freshly polish, immersed in 0.5 M sulfuric acid with 5 mM DLP for 2 hours and surface topography of soaked in 0.5 M sulfuric acid 2 hours, respectively. From Fig. 7(a), the entire surface can be polished very flat, and the scratch after polishing can be clearly seen. Fig. 7(c) clearly shows the voids left behind by the sulfuric acid medium. The entire surface is severely corroded. Fortunately, the surface of the X65 steel in Fig. 7(b) is basically flat and some sanding scratches are faintly visible, indicating that DLP can effectively inhibit the corrosion of X65 steel.

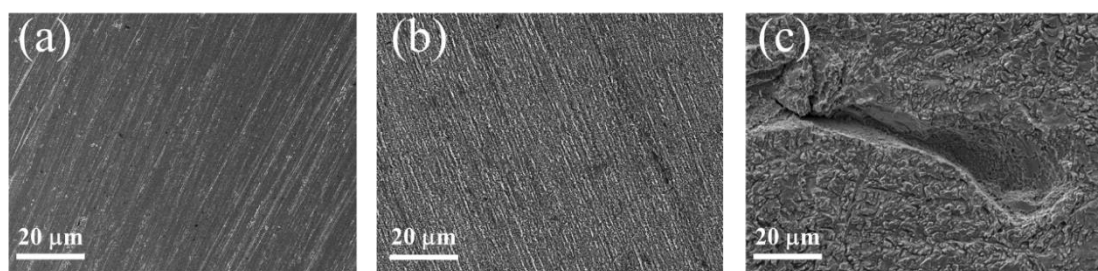


**Figure 7.** Surface topography of X65 steel under different processing conditions at 298 K: (a) newly polished, (b) containing 5 mM DLP soaking for 2 hours, (c) blank solution soaking for 2 hours.

3.5 Atomic Force Microscopy Analysis

Fig.8 is the 3D topography of X65 steel under different conditions, and Fig. 9 is a corresponding contour plots and average roughness values. From Fig. 8(a) and Fig. 9(a), it can be found that the entire steel surface is polished very flat with an average roughness of 7.5 nm.

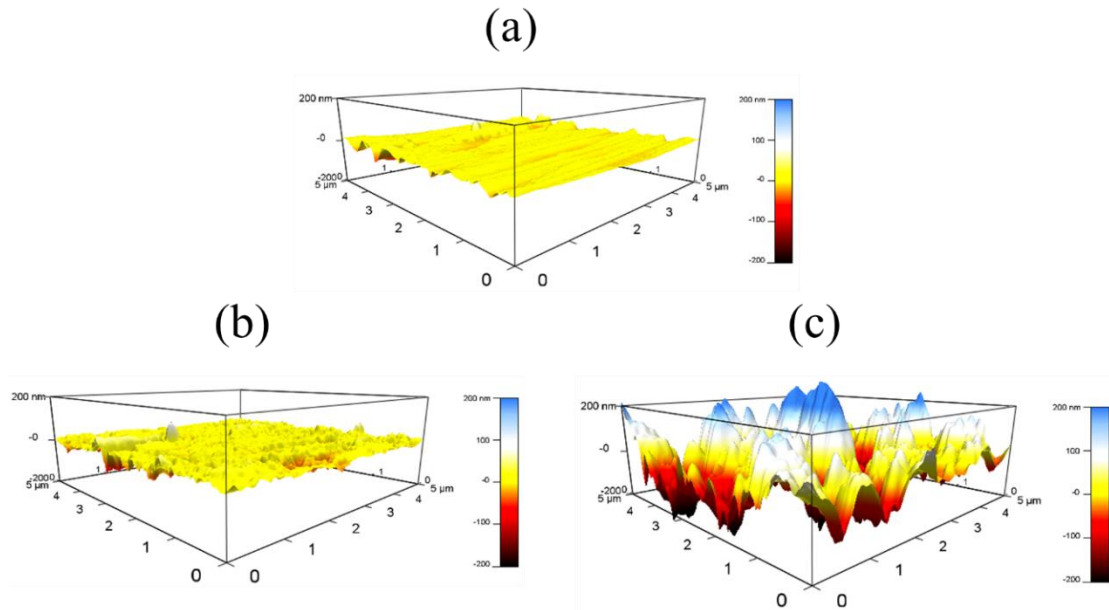


**Figure 8.** 3D topography of X65 steel under different processing conditions at 298 K: (a) newly polished, (b) contains 5 mM DLP soaking for 2 hours, (c) blank solution soaking for 2 hours.

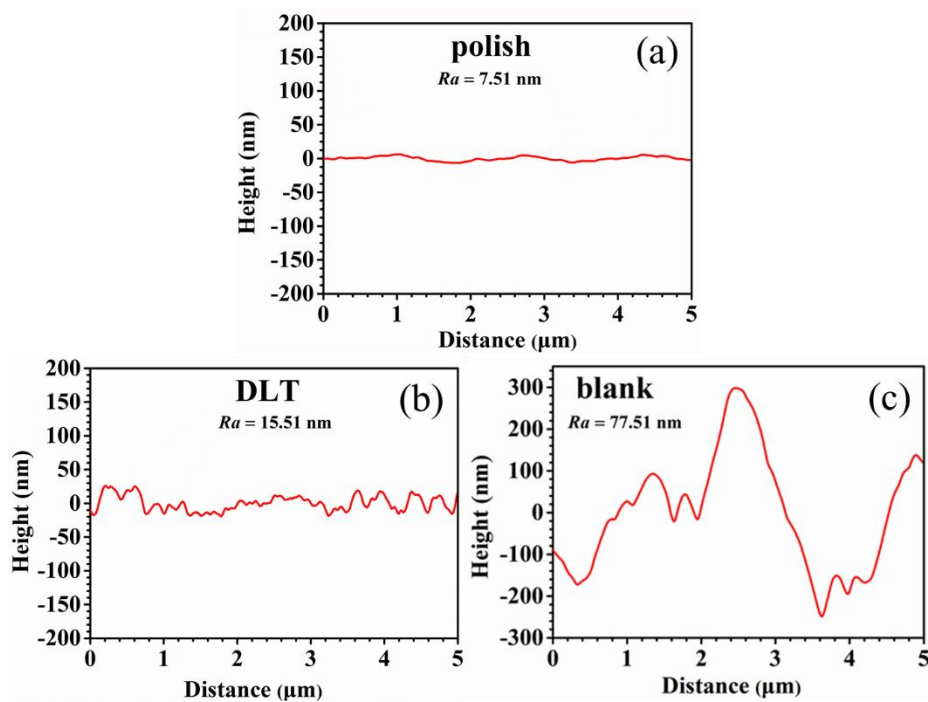


**Figure 9.** Contour plots and average roughness of the X65 steel surface at 298 K: (a) newly polished, (b) 5 mM DLP DLP soaking for 2 hours, (c) blank solution soaking for 2 hours.

Fig. 8 (c) and Fig. 9 (c) correspond to the immersion of X65 steel in a 0.5 M sulfuric acid solution for 2 hours, which the roughness of the entire surface measured is 77.5 nm. Fig. 8 (b) and Fig.9 (b) correspond to immersing X65 steel in a sulfuric acid solution containing 5 mM DLP. The average roughness of the entire steel surface is 15.5 nm. By comparison, it can be found that DLP can effectively inhibit the corrosion of X65 steel in sulfuric acid medium.

### 3.6 Quantum Chemistry Calculation

Structural optimization of DLP molecules and calculation of related quantum chemical parameters were performed on MS software. Fig. 10 shows the molecular configuration of DLP optimization, and the frontier molecular orbital distribution of HOMO and LUMO, respectively. It can be seen from Fig. 10 that the optimized DLP molecules are in a plane, which indicates that the DLP molecules are more adsorbed on the steel surface in a parallel manner. It is worth mentioning that in the DLP molecule, the electron cloud is mainly distributed in the five-membered ring of the S-S single bond, which indicates that the S-S single bond can provide the lone electron pair and the 3d empty orbital formation of Fe in the adsorption process of the steel surface. Thereby effectively adsorbing on the surface of the steel.

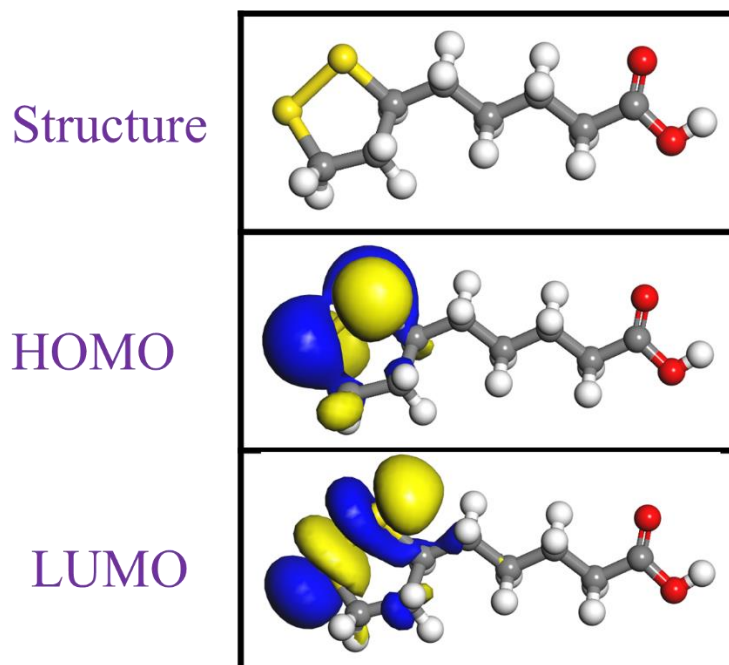


**Figure 10.** The molecular configuration of the DLP optimization, as well as the frontier molecular orbital distribution of HOMO and LUMO, respectively.

In addition, we also calculated the frontier molecular energy and dipole moment of DLT. The HOMO orbital energy of DLP is  $-4.6$  eV, and the energy of LUMO orbit is  $-1.6$  eV. Therefore, the energy gap value of the DLP is  $3.0$  eV ( $E_{LUMO} - E_{HOMO}$ ) [34]. According to the frontier molecular orbital

theory, the molecules corresponding to the HOMO molecular orbital electron-donating ability, and the large value of  $E_{HOMO}$  indicate that the molecule has strong electron-donating ability. The molecular orbital energy of LUMO corresponds to the electron-receiving ability of the molecule. The smaller the value of  $E_{LUMO}$ , the stronger the electron-capable ability of the molecule [35]. DLP molecules have large  $E_{HOMO}$  value, and small  $E_{LUMO}$  value. This shows that it can show excellent corrosion inhibition performance [36]. It is worth mentioning that the DLP molecular dipole moment is 3.8 Debye, which is a larger value in the corrosion inhibitor. In general, large dipole values have the effect of changing the electric double layer capacitance in the vicinity of the electrode, thereby facilitating the adsorption of the corrosion inhibitor molecules on the metal surface [37].

### 3.7 Molecular Dynamics Simulation

The adsorption of DLP molecules on the Fe(110) plane was simulated in MS software, and the optimized stable configuration is shown in Fig. 11. It can be clearly seen from Fig. 11 that the DLP is adsorbed on the surface of Fe(110) in a parallel manner. This adsorption mode is beneficial to the DLP molecule to prevent the corrosion of the X65 steel by the sulfuric acid corrosion medium to the greatest extent. The adsorption energy of DLP in Fe(110) is calculated by the following formulas [38-41]:

$$E_{binding} = -E_{interact} \quad (7)$$

$$E_{interact} = E_{tot} - (E_{subs} + E_{inh}) \quad (8)$$

Among them,  $E_{tot}$  is the total energy of the whole simulation system,  $E_{subs}$  is the energy of the whole simulation system except for the DLP molecule, and  $E_{inh}$  is the energy of the DLP molecule. The calculated adsorption energy was 529 kJ/mol. This large binding energy indicates that the DLP molecule can be effectively adsorbed on the surface of the X65 steel.

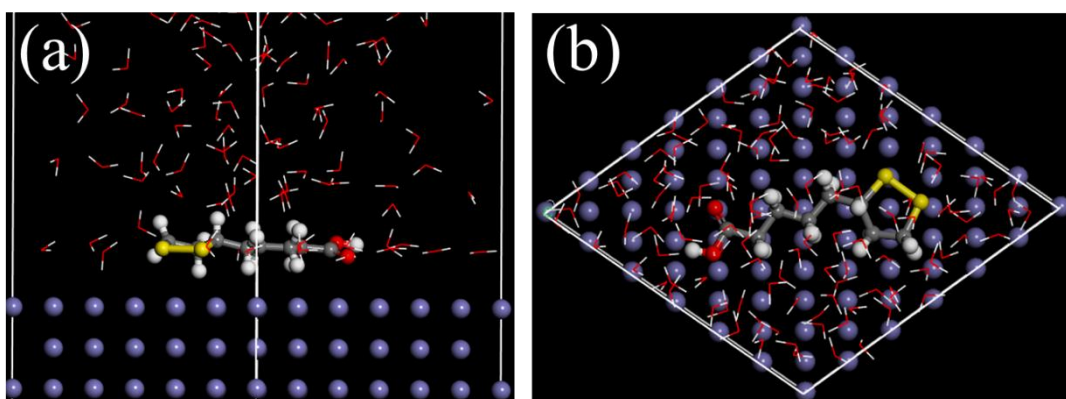


**Figure 11.** Stable configuration of DLP molecules adsorbed on the Fe(110) plane; (a) top view, (b) side view.

## 4. CONCLUSION

The polarization curve indicates that the DLP molecule can effectively reduce the corrosion current density and is a mixed-type corrosion inhibitor that suppresses the anode. Electrochemical

impedance spectroscopy indicates that the adsorption of DLP molecules on the surface of X65 steel causes the charge transfer resistance to increase sharply and the capacitance properties appear, which indicates that the DLP molecules form a dense protective film on X65. The adsorption of DLP on the surface of X65 conforms to the Langmuir adsorption isotherm model and coexists with physicochemical adsorption. The results of the morphology analysis and the electrochemical test are highly consistent. In addition, the theoretical calculation results are consistent with the experimental values.

#### ACKNOWLEDGMENTS

This work was supported financially by Ningbo Natural Science Foundation (2017A610066).

#### References

1. Z. Gong, S. Peng, X. Huang, L. Gao, *Materials*, 11 (2018) 2017.
2. Z.Z. Tasic, M.M. Antonijević, M.B. Petrovic Mihajlovic, M.B. Radovanovic, *J. Mol. Liq.*, 219 (2016) 463.
3. M. A. Albuquerque, Marcia C. C. de Oliveira, Aurea Echevarria, *Int. J. Electrochem. Sci.*, 12 (2017) 852.
4. P. Kannan, T.S. Rao, N. Rajendran, *J. Colloid Interf. Sci.*, 512 (2018) 618.
5. C. Verma, E.E. Ebenso, M.A. Quraishi, *J. Mol. Liq.*, 233 (2017) 403.
6. A.E. Somers, B.R.W. Hinton, C. de Bruin-Dickason, G.B. Deacon, P.C. Junk, M. Forsyth, *Corros. Sci.*, 139 (2018) 430.
7. S. Chen, A. Singh, Y. Wang, W. Liu, K. Deng, Y. Lin, *Int. J. Electrochem. Sci.*, 12 (2017) 782-796.
8. M.P. Casaletto, V. Figà, A. Privitera, M. Bruno, A. Napolitano, S. Piacente, *Corros. Sci.*, 136 (2018) 91.
9. B. Tan, S. Zhang, Y. Qiang, L. Guo, L. Feng, C. Liao, Y. Xu, S. Chen, *J. Colloid Interf. Sci.*, 526 (2018) 268.
10. B. Tan, S. Zhang, H. Liu, Y. Guo, Y. Qiang, W. Li, L. Guo, C. Xu, S. Chen, *J. Colloid Interf. Sci.*, 538 (2019) 519.
11. N. Chen, S. Zhang, Y. Qiang, S. Xu, X. Ren, *Int. J. Electrochem. Sci.*, 11 (2016) 7230.
12. L. Feng, S. Zhang, S. Yan, S. Xu, S. Chen, *Int. J. Electrochem. Sci.*, 12 (2017) 1915-1928.
13. H. Lgaz, R. Salghi, S. Jodeh, B. Hammouti, *J. Mol. Liq.*, 225 (2017) 271.
14. B. Tan, S. Zhang, Y. Qiang, L. Feng, C. Liao, Y. Xu, S. Chen, *J. Mol. Liq.*, 248 (2017) 902.
15. J. Zhang, L. Zhang, G. Tao, *J. Mol. Liq.*, 272 (2018) 369.
16. A. Mishra, C. Verma, H. Lgaz, V. Srivastava, M.A. Quraishi, E.E. Ebenso, *J. Mol. Liq.*, 251 (2018) 317.
17. M. I. Awad, A. F. Saad, M. R. Shaaban, B.A. AL Jahdaly, Omar A. Hazazi, *Int. J. Electrochem. Sci.*, (2017) 1657.
18. M.B. Radovanović, M.M. Antonijević, *J. Adhes. Sci. Technol.*, 31 (2016) 369.
19. G. Bahlakeh, M. Ramezanzadeh, B. Ramezanzadeh, *J. Mol. Liq.*, 248 (2017) 854.
20. M.M. Solomon, S.A. Umoren, *J. Colloid Interf. Sci.*, 462 (2016) 29.
21. J. Haque, V. Srivastava, C. Verma, M.A. Quraishi, *J. Mol. Liq.*, 225 (2017) 848.
22. A. Biswas, P. Mourya, D. Mondal, S. Pal, G. Udayabhanu, *J. Mol. Liq.*, 251 (2018) 470.
23. M. Ramezanzadeh, Z. Sanaei, G. Bahlakeh, B. Ramezanzadeh, *J. Mol. Liq.*, 256 (2018) 67.
24. A.S. Fouda1, M.A. Diab, S. Fathy, *Int. J. Electrochem. Sci.*, 12 (2017) 347.
25. G. Khan, W.J. Basirun, S.N. Kazi, P. Ahmed, L. Magaji, S.M. Ahmed, G.M. Khan, M.A. Rehman, A. Badry, *J. Colloid Interf. Sci.*, 502 (2017) 134.
26. A. Ehsani, M.G. Mahjani, M. Hosseini, R. Safari, R. Moshrefi, H. Mohammad Shiri, *J. Colloid*

- Interf. Sci.*, 490 (2017) 444.
27. S. Mo, H.Q. Luo, N.B. Li, *J. Colloid Interf. Sci.*, 505 (2017) 929.
  28. H. Tian, W. Li, A. Liu, X. Gao, P. Han, R. Ding, C. Yang, D. Wang, *Corros. Sci.*, 131 (2018) 1.
  29. M.I.K. Ismat H. Ali1, *Int. J. Electrochem. Sci.*, 12 (2017) 2285.
  30. K. Zhang, W. Yang, B. Xu, Y. Chen, X. Yin, Y. Liu, H. Zuo, *J. Colloid Interf. Sci.*, 517 (2018) 52.
  31. H. Lgaz, K. Subrahmanya Bhat, R. Salghi, Shubhalaxmi, S. Jodeh, M. Algarra, B. Hammouti, I.H. Ali, A. Essamri, *J. Mol. Liq.*, 238 (2017) 71.
  32. M.A. Deyab, M.T. Zaky, M.I. Nessim, *J. Mol. Liq.*, 229 (2017) 396.
  33. L. Gao, S. Peng, Z. Gong, J. Chen, *RSC Advances*, 8 (2018) 38506.
  34. L.L. Liao, S. Mo, H.Q. Luo, N.B. Li, *J. Colloid Interf. Sci.*, 520 (2018) 41.
  35. M. Abd El-Raouf, E.A. Khamis, M.T.H. Abou Kana, N.A. Negm, *J. Mol. Liq.*, 255 (2018) 341.
  36. K.F. Khaled, *Appl. Surf. Sci.*, 255 (2008) 1811.
  37. S. Issaadi, T. Douadi, S. Chafaa, *Appl. Surf. Sci.*, 316 (2014) 582.
  38. D. Fu, B. Tan, L. Lu, X. Qin, S. Chen, W. He, J. Chen, *Int. J. Electrochem. Sci.*, 13 (2018) 8561.
  39. E. Alibakhshi, M. Ramezanzadeh, G. Bahlakeh, B. Ramezanzadeh, M. Mahdavian, M. Motamedi, *J. Mol. Liq.*, 255 (2018) 185.
  40. S.K.S. Manilal Murmu, Naresh Chandra Murmu, Priyabrata Banerjee, *Corros. Sci.*, 146 (2019) 134.
  41. D. Kumar, V. Jain, B. Rai, *Corros. Sci.*, 142 (2018) 102.

© 2019 The Authors. Published by ESG ([www.electrochemsci.org](http://www.electrochemsci.org)). This article is an open access article distributed under the terms and conditions of the Creative Commons Attribution license (<http://creativecommons.org/licenses/by/4.0/>).